Descriptors of Transition Metal Promoters on MoS2 Nanocatalysts for Hydrodesulfurization: Binding Energy of Metal Sulfides from First Principles

Journal:	*Molecular Systems Design & Engineering*
Manuscript ID	ME-ART-04-2019-000044.R1
Article Type:	Paper
Date Submitted by the Author:	07-Jun-2019
Complete List of Authors:	Joo, Paul; University of California San Diego, Department of NanoEngineering Yang, Kesong; University of California, San Diego, NanoEngineering Department

Design, System, Application Statement

• This work proposes a molecular design and optimization strategy to improve the hydrodesulfurization performance of MoS2 nanocatalysts by selecting most appropriate transition metal promoters, as well as the selection standard based on the effective material descriptor, *i.e.*, binding energy (E_b) of transition metal sulfides.

• This work proposes that desired transition metal promoters for MoS2 nanocatalysts should have neither too large or too small binding energy (Eb) of transition metal sulfides, and in light of this standard, Co, Cr, and Fe are selected as most promising promoters.

• This work provides useful guidance to the design of high-performance MoS2-based nanocatalysts.

Descriptors of Transition Metal Promoters on MoS_2 Nanocatalysts for Hydrodesulfurization: Binding Energy of Metal Sulfides from First Principles

Paul H. Joo[a] **and Kesong Yang**[*a,b]

Received Xth XXXXXXXXXX 20XX, Accepted Xth XXXXXXXXX 20XX
First published on the web Xth XXXXXXXXXX 200X
DOI: 10.1039/b000000x

MoS_2-based catalysts have been used in the petroleum refinery industry for decades and it is of long-term interests to improve their catalytic efficiency in hydrodesulfurization (HDS) process such as via edge promotion using transition metal (TM) atoms. To develop an effective descriptor for selecting appropriate TM promoters, here we report a comprehensive computational study of TM promotion effects on the catalytic activity of MoS_2 nanosheets with 26 TM elements, including ten 3*d*, eight 4*d*, and eight 5*d* elements, using sulfur-terminated hexagonal MoS_2 nanosheets. The binding energies between TM atoms and MoS_2 nanosheets without and with sulfur saturation and the formation energies of sulfur vacancies of the TM-promoted MoS_2 promoters were studied to examine the possibility of edge promotion of TM atoms. The HDS activity of sulfur saturated TM-MoS_2 nanocatalysts is evaluated by modeling three consequent steps in an HDS process with a dibenzothiophene molecule. We calculated the reaction energy for each step with respect to the binding energy ($E_b \sim$ 2.5 - 6.5 eV/atom) of binary TM sulfides and found that E_b can be an effective descriptor for selecting TM promoters to enhance the catalytic activity of MoS_2 nanocatalysts. That is, E_b of an ideal TM promoter should neither be extremely high nor extremely low with an ideal range about 4 - 5 eV/atom. On the basis of this descriptor, several candidate TM promoters including 3*d* elements Mn, Cr, Co, Fe, Ni, and V, 4*d* element Ru, and 5*d* element Pt are proposed. This work is expected to provide an informative guide to the design of high-performance MoS_2-based nanocatalysts for HDS.

1 Introduction

The hydrodesulfurization (HDS) plays a critical role in producing clean diesel fuel from the crude oil.[1–8] As the demand for the ultra-low sulfur diesel grows, transition metal sulfides (TMS)-based catalysts have gained a prominent interest because of their applications in the HDS processes.[9–12] As one TMS-based nanocatalyst, single-layer molybdenum disulfide (MoS_2) has been extensively studied.[13,14] For decades, there have been tremendous efforts on the structural identifications of single-layer MoS_2 and the elucidation into the effects of nanostructures on the catalytic properties.[15–18] It is now known that single-layer MoS_2 exists in multiple shapes, depending on its growth conditions.[15–17] The shape of single-layer MoS_2 undergoes an evolution from dodecagonal to hexagonal, and to triangular from sulfur-poor to sulfur-rich growth conditions.[15,19] Under sulfur-rich condition, triangular MoS_2 layers were observed using scanning tunneling microscopy (STM)[20] and transmission electron microscopy (TEM)[21] in the experimental side. In the theoretical and computational side, our previous study revealed an odd-even effect of the formation of sulfur vacancies in the triangular MoS_2 nanosheets with respect to size,[22] which is consistent with the experimental findings.[16,20] Under sulfur-poor condition, Co-Mo-S structures were found in a hexagonal shape *via* an STM analysis,[3] and a Co promotion on the MoS_2 nanoclusters also lead to a hexagonal nanocluster under the HDS environment.[23]

To improve the catalytic efficiency of MoS_2, several methods including the synthesis of various nanostructures, fabrication of heterostructures, and edge-promotion *via* TM atoms, have been explored.[24–27] For instance, MoS_2 nanotubes show enhanced catalytic activity due to large surface exposure, with approximately 19% of conversion efficiency of dibenzothiophene (DBT) to biphenyl (BP).[24] The Co_3S_4@MoS_2 heterostructures exhibited an enhanced catalytic activity due to abundant electrochemical surfaces and modulated coordinations in the electrocatalytic hydrogen evolution reaction.[27] In particular, TM promotion on the edges of MoS_2 nanosheets is one effective way to improve the catalytic activity because it increases the number of active catalytic sites,[25,28] *i.e.*, the adsorption site that attracts and converts the organic compounds

[a] *Program of Materials Science and Engineering, University of California San Diego, La Jolla, CA 92093-0418, USA.*
[b] *Department of NanoEngineering, University of California, San Diego, La Jolla, CA 92093-0448, USA.*
[*] *Tel: +1-858-534-2514; E-mail: kesong@ucsd.edu*

into clean diesel fuel compounds.[18,25,26] As a proof of the concept, Co- and Ni-promoted MoS_2 showed a conversion efficiency of 97.8% and 94%, respectively, in the HDS reaction of thiophene under 375°C.[25] Co-promoted MoS_2 nanosheets with a better Co dispersion over the edges were also found to show a better catalytic activity.[28] Besides Co,[29–33] some other TM promoters including Ni,[29–31] and Fe[29,32] have also been explored in the experimental side. However, the effects of various TM promoters on the HDS activity of MoS_2 nanocatalysts are not fully understood yet from the theoretical side. For instance, one might wonder which TM promoter can best improve the HDS activity of MoS_2 nanocatalysts and what alternative TM promoters can be used, and to answer this question, a systematic comparison of the promotion effects, regarding thermochemistry, of various TM atoms on the MoS_2 nanocatalysts is necessary.

In this work, using first-principles density functional theory calculations, we studied the effects of 26 TM elements, as a promoter on the hexagonal MoS_2 nanosheets, on the catalytic activity in the HDS process. The article is organized as follows. First, we discussed the energetic stability of the TM-promoted MoS_2 nanosheets by calculating the binding energies. Next, we calculated the formation energies of sulfur vacancy on the promoted edge of the nanosheets. Lastly, we evaluated the catalytic activity by calculating reaction energies in the HDS process. Our results show that the binding energy of TM sulfides could be one effective descriptor for selecting TM promoters for the MoS_2 nanocatalyst to optimize catalytic activity for HDS.

2 Computational Details

First-principles density functional theory (DFT) electronic structure calculations were carried out using the Vienna *Ab initio* Simulation Package (VASP).[34,35] The Projector Augmented Wave (PAW) potential was employed for treating electron-ion interactions[36] and the Generalized Gradient Approximation (GGA) parameterized by Perdew-Burke-Ernzerhof (PBE) was applied for the electron-correlation functional.[37] A cut-off energy of 450 eV for the plane-wave basis set, a convergence tolerance of 10^{-4} eV for the self-consistent-field iteration, and a single *k*-point with wavevector at Γ point were used in our calculations. The atomic positions of the MoS_2 nanosheets were fully relaxed until all components of the residual forces became less than 0.05 eV/Å. To model the hydrodesulfurization process, the Grimme's D3 dispersion correction on the PBE functional (PBE+D3) was employed to calculate the chemical reaction energies between the organosulfur compounds and MoS_2 nanosheets, since it is capable of predicting more accurate thermochemical energy.[38] The zero-point energy (ZPE) correction to the adsorbed molecules were calculated from the harmonic frequency of the molecules absorbed on the MoS_2 nanosheets.[39,40]

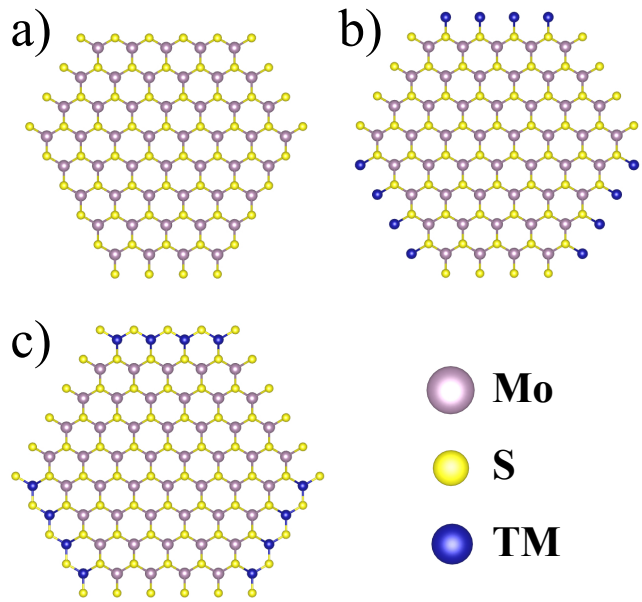

Fig. 1 Schematic illustration of single-layer hexagonal MoS_2 nanosheet structures. (a) Unpromoted and (b) promoted with transition-metal (TM) atoms without and (c) with sulfur saturation.

A single-layer MoS_2 nanosheet structure consists of one Mo layer and two S layers, with the Mo layer sandwiched by the two S layers. In our prior work, we defined two types of zigzag edges for MoS_2 nanosheet structure, including ZZ-S1 and ZZ-S2.[22] The ZZ-S1 edge has a S-termination, with each S dimer coordinatively bonded to two Mo atoms. The ZZ-S2 edge also has a S-termination, but with S dimers protruding externally in a perpendicular direction from the edges.[22] In the experiment, MoS_2 nanoclusters were observed in a hexagonal shape with exposures of both promoted ZZ-S1 edges and unpromoted ZZ-S2 edges upon Co promotion.[14,19,23,30,41] Accordingly, in this work, we built a hexagonal MoS_2 nanosheet model with three ZZ-S1 and three ZZ-S2 edges to resemble the experimental nanosheet structure, see Fig. 1a. To eliminate the interaction between neighboring slabs, a vacuum region of 10 Å was applied in our models. Based on the growth conditions of the MoS_2 nanosheet and inspired by prior experimental studies,[42] we built another two models for the TM promotion, including one without sulfur saturation (see Fig. 1b) and the other with sulfur saturation (see Fig. 1c). The promoted MoS_2 model was built by promoting S dimers of the three ZZ-S1 edges with TM atoms which share the same layer with Mo atoms. The TM atoms including ten 3*d*, eight 4*d*, and eight 5*d* elements were selected. In the case of TM-promoted model with sulfur saturation, S monomers are at-

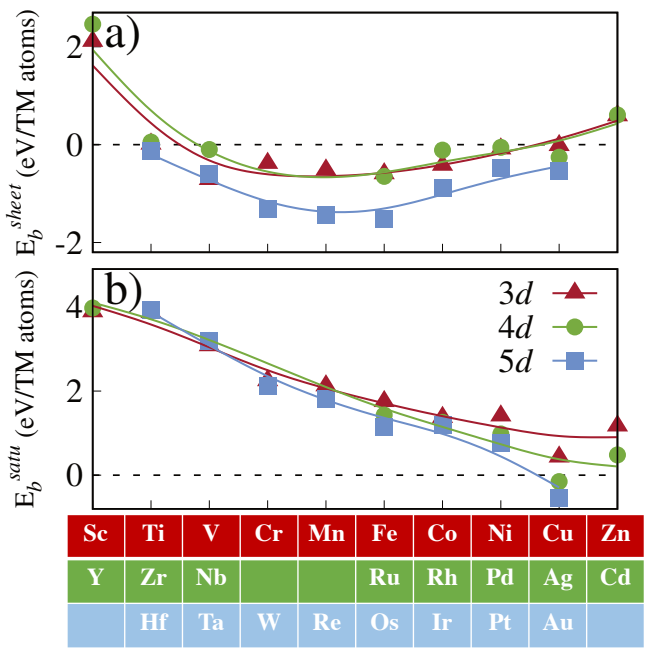

Fig. 2 Calculated binding energies of TM-promoted MoS_2 nanosheets a) without and b) with sulfur saturation. The chemical potentials of TM and sulfur atoms calculated from their ground state bulk structures were used in this and subsequent figures.

tached on the TM atoms in the same layer, in a similar manner of ZZ-S1 type edge. Such model resembles the Co-[18,31,43] and Ni-[31] promoted MoS_2 nanosheets observed in the experiments.

3 Results and Discussion

3.1 Binding Energy

To quantitatively evaluate the binding strength between TM atoms and MoS_2 nanosheets, we first calculated the binding energies (E_b^{sheet}) of the TM-promoted MoS_2 nanosheets without sulfur saturation using the formula:

$$E_b^{sheet} = [E_{unprom} + x\mu_{TM} - E_{prom}]/x \quad (1)$$

where x and μ_{TM} are the total number and the chemical potential of the TM atom, respectively. E_{unprom} and E_{prom} indicate the total energy of the unpromoted and promoted hexagonal MoS_2 nanosheets, respectively. The calculated binding energies for these TM-promoted MoS_2 nanosheets are shown in Fig 2a. The binding energy can be interpreted as the energy required for the TM atoms to detach from the MoS_2 nanosheets. Our results show a negative binding energy for most of TM-MoS_2 nanosheets except for Sc-, Y-, Zn-, and Cd-MoS_2. The negative binding energy indicates a spontaneous dissociation of the TM atoms from the MoS_2 nanosheet, which implies that TM promotion on the nanosheet without sulfur saturation is not energetically possible.

Next, we calculated the binding energy (E_b^{satu}) of the TM-promoted model with sulfur saturation using the equation:

$$E_b^{satu} = [E_{unprom} + x\mu_{TM} + y\mu_S - E_{satu}]/x \quad (2)$$

where E_{satu} is the total energy of the sulfur saturated TM-MoS_2, μ_{TM} and μ_S are the chemical potentials of the TM and S atom, respectively, and x and y are total number of the TM atoms and the saturating S atoms on the promoted edges, respectively. Note that the label E_b^{satu} was used to differentiate the binding energy of TM-promoted MoS_2 model with sulfur saturation from the MoS_2 nanosheets without sulfur saturation (E_b^{satu}) and the transitional metal sulfides (E_b). The calculated binding energies of the TM-promoted MoS_2 nanosheets with sulfur saturation are plotted in Fig. 2b. Our calculations reveal two major conclusions:

1) All TM-MoS_2 nanosheets have a positive binding energy, except for Ag- and Au-MoS_2. This indicates the feasibility of the TM promotion on the MoS_2 nanosheet under the sulfur saturating condition as compared to the infeasibility under unsaturating condition. This is also consistent with a prior experimental study in which Co-promoted MoS_2 was observed under sulfur saturating condition from STM images.[23]

2) The binding energy decreases along the groups in the periodic table for each of the 3*d*, 4*d*, and 5*d* TM elements. The TM atoms from group 3 (Sc and Y) and group 4 (Ti, Zr, and Hf) lead to the higher binding energy, while the TM atoms from group 11 (Cu, Ag, and Au) and group 12 (Zn and Cd) lead to the lower binding energy. This can be explained from the electronegativity of the TM elements. For the TM elements with low electronegativity (high electropositivity) in the lower groups of periodic table, they tend to cause strong binding with S atom. For the TM elements with high electronegativity (low electropositivity) in the high groups of periodic table, they tend to have weaker binding with the S atom.

3.2 Formation Energy of Sulfur Vacancy

Next, we calculated the formation energy of sulfur vacancy on the TM-MoS_2 nanosheets with sulfur saturation. This is because the sulfur vacancy site is considered as an active site and plays a critical role in the HDS reaction by attracting the organosulfur compounds. The sulfur vacancy site is also called the coordinatively unsaturated site (CUS),[22] which has been spotted *via* STM images in the experiment.[44] In this work, the sulfur vacancy (V_S) was modeled by removing one sulfur monomer from the center site of the TM-promoted edge (V_S@Cen). The formation energy of V_S@Cen was calculated using the equation,

$$E_f = E_{V_S@Cen} + \mu_S - E_{satu} \quad (3)$$

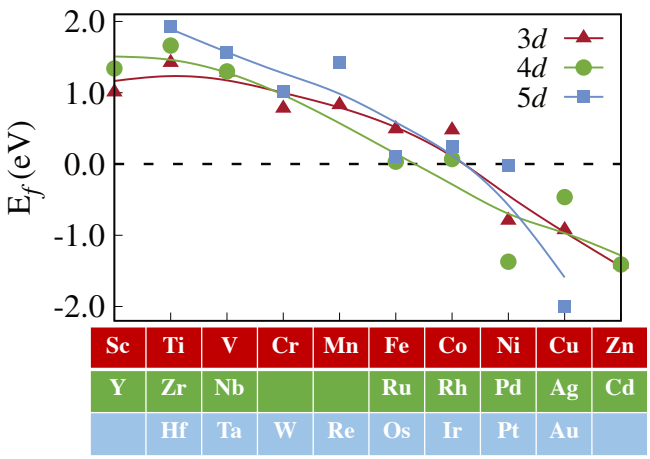

Fig. 3 Calculated formation energies of TM-promoted MoS_2 nanosheets with sulfur vacancy at the center site of the saturated edge (V_S@Cen) at sulfur-poor condition.

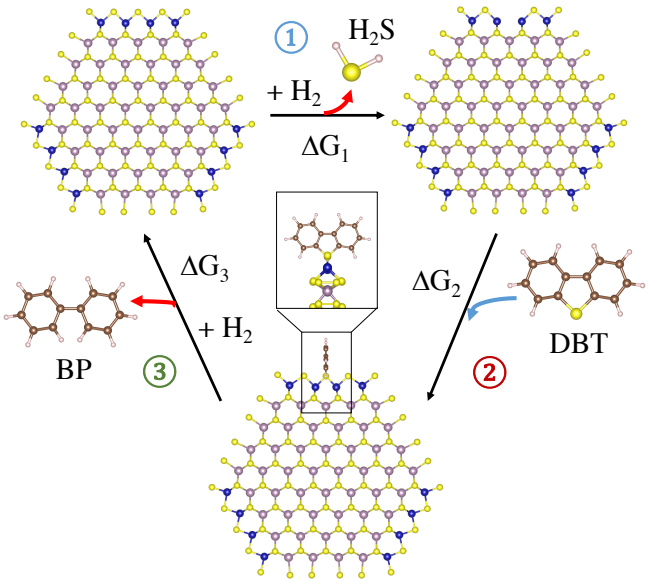

Fig. 4 The schematic diagram of the hydrodesulfurization reaction of dibenzothiophene (DBT) to biphenyl (BP) with TM-MoS_2 nanosheet. (1) Generation of sulfur vacancy at the center site of the edge (V_S@Cen), (2) Adsorption of DBT, and (3) Desulfurization of DBT into BP. The blue arrow indicates the incoming reactant in the reaction, while the red arrow indicates the release of a product in the reaction.

where $E_{V_S@Cen}$ is the total energy of the V_S@Cen and μ_S is the chemical potential of the S atom.

The calculated formation energies of V_S@Cen are depicted in Fig. 3. It shows that the formation energy, generally, decreases from group 3 to group 12 for all rows of 3*d*, 4*d*, and 5*d* TM elements, indicating that V_S@Cen is energetically more favorable in the systems with TM promoters in the higher groups of periodic table. Interestingly, the V_S@Cen for Ni-, Cu-, Zn-, Pd-, Ag-, Cd-, and Au-MoS_2 nanosheets have a negative formation energy (-0.79, -0.93, -1.41, -1.37, -0.46, -1.41, and -2.00 eV, respectively), which indicates a spontaneous formation of V_S@Cen. This can directly relate to the decreasing trend in the binding energy (E_b) for TM-sulfides, shown in Fig. S4 in the Supporting Information. In general, E_b decreases with the TM atoms from group 3 to group 12. ScS and TiS have a relatively high E_b of 5.63 and 5.74 eV/atom, respectively, while ZnS has a relatively low E_b of 2.99 eV/atom, as shown in Table S1. A lower E_b means weaker binding strength between the TM and S atoms, thus leading to a relatively easier formation of V_S.

In fact, the decrease in the formation energy of V_S@Cen can also relate to the decrease in the binding energy of the TM-MoS_2 with sulfur saturation (Fig. 2b), because such binding energy also reflects on the binding strength between the TM and S atoms. However, their difference is that the V_S@Cen formation accounts for the interaction between the TM atoms and the S monomers that lie on top of the promoted TM atoms, while the binding energy of the TM-MoS_2 with sulfur saturation refers to the interaction between the TM atoms and the S dimers that connect the TM atoms to the MoS_2 nanosheet.

3.3 Hydrodesulfurization Modeling

The HDS process consists of three consequent steps: (1) generation of V_S, (2) adsorption of a S-containing organic molecule into the V_S site of the catalyst via the S atom, and (3) desulfurization of the organic molecule with S refilling the V_S site. The schematic diagram of the HDS process is shown in Fig. 4. Dibenzothiophene (DBT) is a typical natural-occurring organosulfur compound in petroleum.[45] Here, we modeled the HDS by using the DBT molecule as a feed compound which becomes a biphenyl (BP) after the HDS reaction. The attachment of DBT to the V_S@Cen site was modeled in a perpendicular orientation to minimize steric hindrance. To evaluate HDS activity of TM-MoS_2 nanosheets, we calculated the Gibbs free energies for each of reaction (1), (2), and (3) using the following equations by taking zero-point energy and entropy corrections into account, respectively:

$$\Delta G_1 = \Delta E_1 - \Delta E_{ZPE}(H_2) - \Delta E_{ZPE}(H_2S) - T(\Delta S_{H_2S} - \Delta S_{H_2}) \quad (4)$$

$$\Delta G_2 = \Delta E_2 + \Delta E_{ZPE}(DBT) + T\Delta S_{DBT} \quad (5)$$

$$\Delta G_3 = \Delta E_3 - \Delta E_{ZPE}(H_2) - \Delta E_{ZPE}(BP) - T(\Delta S_{BP} - \Delta S_{H_2}) \quad (6)$$

where ΔE_1, ΔE_2, and ΔE_3 are the reaction energies in reaction (1), (2), and (3), respectively; $\Delta E_{ZPE}(H_2)$, $\Delta E_{ZPE}(H_2S)$, ΔE_{ZPE}(DBT), and ΔE_{ZPE}(BP) and ΔS_{H_2}, ΔS_{H_2S}, ΔS_{DBT}, and ΔS_{BP} are the difference in zero-point energy and entropy of H_2, H_2S, DBT, and BP between their adsorbed states and their isolated states, respectively. The room temperature 298 K was used in calculations. The difference in entropy are obtained from $S^o_{H_2S}$[46], $S^o_{H_2}$[46], S^o_{DBT}[47], and S^o_{BP}[48], respectively, based on the assumption that the vibrational entropy in their adsorbed states is small.[49] The calculated difference in zero-point energy and entropy is listed in the Table S1 of Supporting Information for reference. Also note that the magnitudes of $\Delta E_{ZPE}(H_2)$ in equations (4) and (6) are slightly different since their absorbed states are different, with MoS_2 and BP being as their absorbing systems, respectively. The reaction energies for reaction (1), (2), and (3) can be calculated using the following equations, respectively:

$$\Delta E_1 = E_{V_S@Cen} + E_{H_2S} - E_{MoS_2} - E_{H_2} \quad (7)$$

$$\Delta E_2 = E_{DBT-MoS_2} - E_{V_S@Cen} - E_{DBT} \quad (8)$$

$$\Delta E_3 = E_{MoS_2} + E_{BP} - E_{DBT-MoS_2} - E_{H_2} \quad (9)$$

where E_{MoS_2}, E_{H_2S}, and E_{H_2} are the total energy of TM-MoS_2 (equivalent to $E_{saturated}$), H_2S, and H_2, respectively, and $E_{DBT-MoS_2}$, E_{DBT}, and E_{BP} are the total energy of DBT-adsorbed TM-MoS_2, DBT, and BP, respectively. The ΔG_1, ΔG_2, and ΔG_3 are plotted against the calculated binding energy (E_b) of binary transition-metal sulfides in Fig. 5a, b, and c, respectively. There are two reasons to choose E_b as a descriptor: i) E_b generally measures the bonding strength between the TM and S atoms, which is strongly correlated to the formation of V_S and chemical adsorption of the DBT via TM-S bond. ii) E_b is a relatively simple parameter that can be accessed from both experiments and theoretical calculations. Actually, earlier experimental and theoretical studies both indicate a correlation between the trends of the HDS activity and the binding energy of sulfur to the transition metals (or the positions of the metals in the periodic table).[13,50]

The 3*d*, 4*d*, and 5*d* TM promoters are depicted as red triangle, green circle, and blue square points, respectively. The calculated E_b is listed in Table S2 for reference.

The ΔG_1 in Fig. 5a represents the reaction energy of V_S@Cen under the H_2 exposure. It shows that ΔG_1 increases as E_b increases, meaning that more energy is required to create V_S@Cen. In contrast, a lower E_b leads to a relatively lower ΔG_1, indicating an easier formation of V_S@Cen. In fact, the negative ΔG_1 for Cu-, Ni-, Zn-, Pd-, Cd-, Ag-, and Au-MoS_2 nanosheets indicates spontaneous formation of V_S@Cen.

The ΔG_2 in Fig. 5b represents the reaction energy of DBT adsorbing into the V_S@Cen of the TM-MoS_2 nanosheet. For MoS_2 with 3*d* TM promoters, ΔG_2 first decreases even to negative values, then increases as E_b increases. A negative value indicates that this reaction is exothermic and spontaneous. The primary decrease in ΔG_2 can be explained by a strong binding strength between the TM atoms and the S atom as indicated by high E_b. A lower and negative ΔG_2 means that more energy is released for the adsorption of DBT to the MoS_2 nanosheet and therefore, it can also be interpreted as a stronger adsorption of DBT. Interestingly, ΔG_2 starts to increase as E_b increases over ~4.75 eV/atom. To understand this behavior, we studied the charge distribution among the S atoms upon DBT adsorption by calculating the difference of Bader charge (ΔC) between the S atom from DBT (S_C) and the two adjacent S atoms (S_L and S_R) from the MoS_2 nanosheet using the equation:

$$\Delta C = \frac{S_L + S_R}{2} - S_C \quad (10)$$

Fig. 5d represents the plotted ΔC as a function of E_b. Note that ΔC is larger than zero, which refers to more charge migration towards S_L and S_R rather than S_C. Interestingly, ΔC shows a similar trend with ΔG_2. That is, ΔC decreases first, then increases with respect to E_b. The decrease in ΔC indicates that less charge is transferred towards S_L and S_R, suggesting that there is a more comparable charge distribution among the S atoms, implying a strong chemical absorption of DBT to the MoS_2. In contrast, the increase in ΔC at relatively high E_b means more charge migration towards S_L and S_R while less charge migration toward S_C. This indicates a weak binding strength between the TM atoms and S_C, thus leading to an increase of ΔG_2. The 4*d* TM promoters, generally, result in a low ΔG_2 at high E_b, which can be simply related to a strong TM-S bonding strength. The 5*d* TM promoters tend to have a consistent ΔG_2.

The ΔG_3 in Fig. 5c represents the reaction energy required to produce BP and regenerate TM-MoS_2 by refilling the V_S@Cen site with the S atom from DBT. As E_b increases, ΔG_3 decreases, which means less energy is required to refill the V_S@Cen site. In fact, the negative ΔG_3 indicates a spontaneous reaction. A higher E_b indicates a stronger binding strength between the TM and the S atoms and therefore, leads to a relatively easier refilling of the V_S@Cen site.

For a clear comparison, the corresponding ΔG_1, ΔG_2, and ΔG_3 for the unpromoted MoS_2 nanosheet were also calculated, shown by the dashed lines in Fig. 5a, b, and c, respectively. Here, the V_S@Cen was modeled by removing one sulfur atom from the sulfur dimer located at the center of the edge of the unpromoted nanosheet, as in the case of TM-promoted MoS_2. It is clear that step (1) occurs spontaneously, as indicated by the negative values of ΔG_1. The TM promotion improves the refilling of the V_S@Cen site in step (3) for most of the TM atoms, as indicated by the lower value

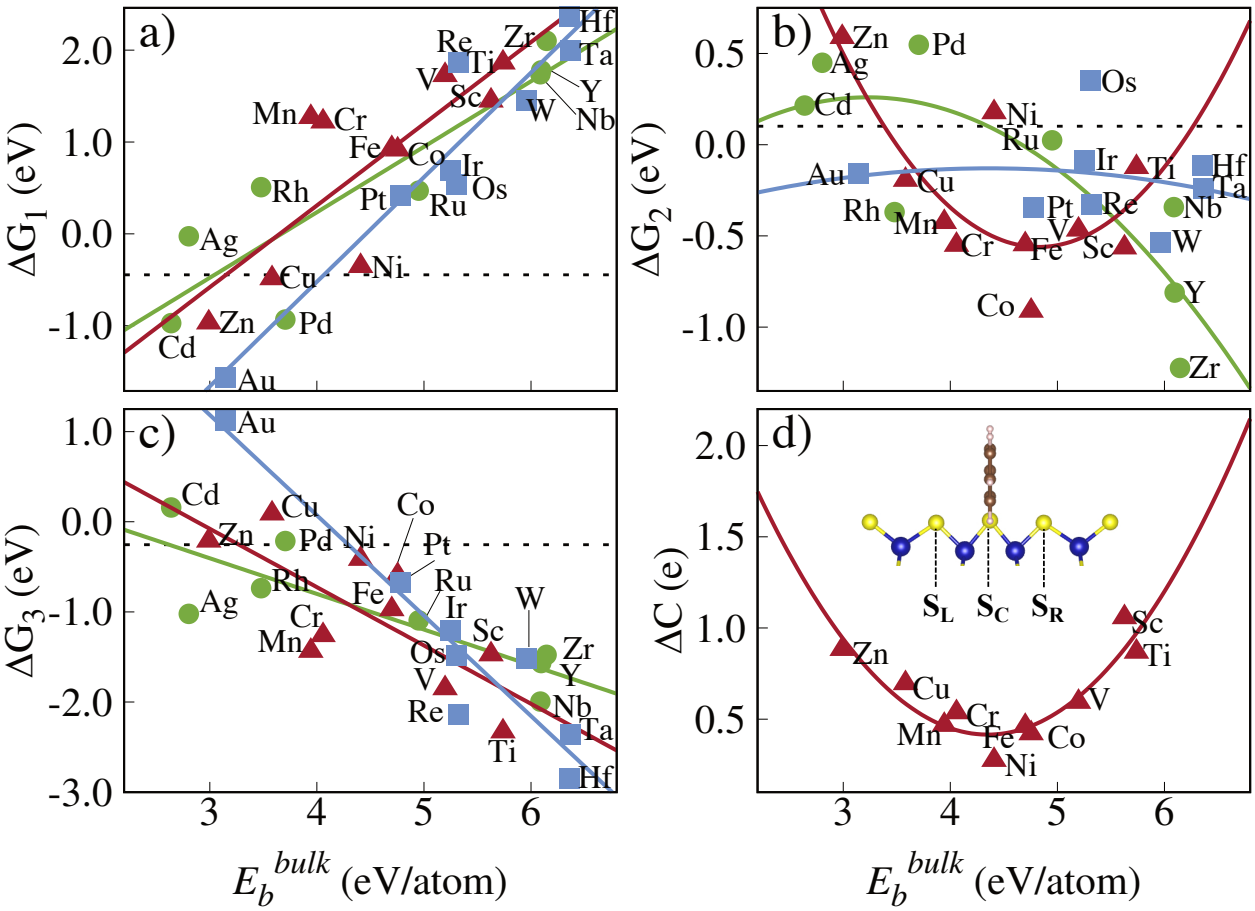

Fig. 5 Calculated reaction energies, a) ΔG_1, b) ΔG_2, and c) ΔG_3 with respect to the binding energy (E_b) of each corresponding TM-sulfides, d) the plotted Bader charge difference (ΔC) between the transferring S atom (S_C) and the adjacent S atoms (S_L and S_R). The 3*d* promoters are in red triangle, 4*d* promoters in green circle, and 5*d* promoters in blue square points. The dashed lines indicate the Gibbs free energies of the reactions with the unpromoted MoS_2 nanosheet.

of ΔG_3 compared to the unpromoted nanosheet. Finally, the relatively high value of ΔG_2 for the unpromoted MoS_2 indicate that most of the TM promoters cause stronger adsorption of DBT than the unpromoted one, emphasizing the improvement of the HDS activity by TM promotion.

As mentioned above, the HDS process is composed of three consequent steps, which involves three parameters, ΔG_1, ΔG_2, and ΔG_3. The ΔG_1 describes the energy required for the formation of V_S@Cen and thus, a lower ΔG_1 is desirable for step (1). The ΔG_2 evaluates the tendency to adsorb DBT *via* the V_S@Cen site and thus, a lower ΔG_2 is desirable for step (2). The ΔG_3 means the reaction energy required to refill the V_S@Cen site and produce BP and thus, a lower ΔG_3 is desirable for step (3). It is worth mentioning that the total change of free energies ($\Delta G = \Delta G_1 + \Delta G_2 + \Delta G_3$) in all three steps is about -0.60 eV, which does not depend on the choice of TM promoters. However, by combining the three steps and the trends of the three parameters as E_b, we are able to conclude that an ideal TM promoter should neither be extremely high or extremely low E_b for its corresponding TM sulfides. This is also consistent with the Sabatier principle, that is, the interaction between the catalyst and the substrate should neither be too strong nor too weak.[51,52] In other words, the E_b can be considered as one effective descriptor for selecting TM promoters. On the basis of this descriptor, we are able to identify several promising TM promoters including 3*d* elements Mn, Cr, Co, Fe, Ni, and V, 4*d* element Ru, and 5*d* element Pt for enhancing the catalytic performance in the HDS process, with neither too strong nor too weak bonding interaction with S, as shown in Fig. 5. This is in good agreement with prior experimental findings that highlight the potential of 3*d* elements Cr,[53,54] Mn,[55] Fe[53], Co[31,33,56,57] and Ni,[29–31] 4*d* element Ru[58] as promoters of MoS_2 catalyst for HDS reaction. Interestingly, recent studies also indicate that the 3*d* element

V[59] or 5*d* element Pt[60] can be appropriate promoters for improving catalytic activity of MoS_2 in the oxygen reduction reaction and hydrogen evolution reaction, respectively, which is consistent with our prediction.

4 Conclusions

In summary, we have studied TM promotion effects on the HDS activity of MoS_2 nanocatalysts using first-principles density functional theory calculations. Our results show that sulfur saturation is necessary for the TM promotion on MoS_2 nanosheets, and if without sulfur saturation, most TM atoms are unable to be attached on the nanosheets. The calculated formation energies of sulfur vacancy decrease with the TM promoters from group 3 to group 12 in the periodic table. This can be related to the decrease of the binding strength between the TM and S atoms, which is represented by the binding energy (E_b) of the binary TM sulfides. By modeling the three separate steps in the HDS process with a DBT molecule, we calculated the reaction energies for each step and revealed that E_b can be an effective descriptor for selecting TM promoters. That is, an ideal TM promoter should have neither extremely low nor extremely high E_b for its corresponding TM sulfide. On the basis of this finding, we propose several candidate TM promoters including 3*d* elements Mn, Cr, Co, Fe, Ni, and V, 4*d* element Ru, and 5*d* element Pt to enhance the catalytic performance of MoS_2 nanocatalysts.

5 Acknowledgment

Acknowledgment is made to the Donors of the American Chemical Society Petroleum Research Fund for support of this research under the award number 55481-DNI6. This work used the Extreme Science and Engineering Discovery Environment (XSEDE), which is supported by National Science Foundation grant number OCI-1053575. The authors thank Dr. Jianli Cheng and Mr. Sicong Jiang for useful discussions.

References

1 R. G. Leliveld and S. E. Eijsbouts, *How a 70-year-Old Catalytic Refinery Process is Still Ever Dependent on Innovation*, Catal. Today **130**, 183–189 (2008).

2 R. R. Chianelli, M. H. Siadati, M. Perez De la Rosa, G. Berhault, J. P. Wilcoxon, R. Bearden Jr., and B. L. Abrams, *Catalytic Properties of Single Layers of Transition Metal Sulfide Catalytic Materials*, Cat. Rev.-Sci. Eng. **48**, 1–41 (2006).

3 F. Besenbacher, M. Brorson, B. S. Clausen, S. Helveg, B. Hinnemann, J. Kibsgaard, J. V. Lauritsen, P. G. Moses, J. K. Nørskov, and H. Topsøe, *Recent STM, DFT and HAADF-STEM Studies of Sulfide-Based Hydrotreating Catalysts: Insight into Mechanistic, Structural and Particle Size Effects*, Catal. Today **130**, 86–96 (2008).

4 C. Song, *An Overview of New Approaches to Deep Desulfurization for Ultra-Clean Gasoline, Diesel Fuel and Jet Fuel*, Catal. Today **86**, 211–263 (2003).

5 C. Song and X. Ma, *New Design Approaches to Ultra-Clean Diesel Fuels by Deep Desulfurization and Deep Dearomatization*, Appl. Catal. B: Environ. **41**, 207–238 (2003).

6 T. A. Saleh, *Simultaneous adsorptive desulfurization of diesel fuel over bimetallic nanoparticles loaded on activated carbon*, J. Clean. Prod. **172**, 2123 – 2132 (2018).

7 T. A. Saleh, *Advanced nanomaterials for water engineering, treatment, and hydraulics*, Advances in environmental engineering and green technologies (AEEGT) (IGI Global, 2017).

8 T. A. Saleh and V. Gupta, *Nanomaterial and Polymer Membranes* (Elsevier, 2016), 1 edn.

9 M. Šarić, P. G. Moses, and J. Rossmeisl, *Relation between Hydrogen Evolution and Hydrodesulfurization Catalysis*, ChemCatChem **8**, 3334–3337 (2016).

10 H. A. Al-Jamimi, A. Bagudu, and T. A. Saleh, *An intelligent approach for the modeling and experimental optimization of molecular hydrodesulfurization over AlMoCoBi catalyst*, J. Mol. Liq. **278**, 376 – 384 (2019).

11 T. A. Saleh, S. A. AL-Hammadi, and A. M. Al-Amer, *Effect of boron on the efficiency of MoCo catalysts supported on alumina for the hydrodesulfurization of liquid fuels*, Process Saf. Environ. **121**, 165 – 174 (2019).

12 T. A. Saleh, S. A. AL-Hammadi, I. M. Abdullahi, and M. Mustaqeem, *Synthesis of molybdenum cobalt nanocatalysts supported on carbon for hydrodesulfurization of liquid fuels*, J. Mol. Liq. **272**, 715 – 721 (2018).

13 T. A. Pecoraro and R. R. Chianelli, *Hydrodesulfurization Catalysis by Transition Metal Sulfides*, J. Catal. **67**, 430–445 (1981).

14 B. Hinnemann, P. G. Moses, and J. K. Nørskov, *Recent Density Functional Studies of Hydrodesulfurization Catalysts: Insight into Structure and Mechanism*, J. Phys.: Condens. Matter **20**, 064236 (2008).

15 D. Cao, T. Shen, P. Liang, X. Chen, and H. Shu, *Role of Chemical Potential in Flake Shape and Edge Properties of Monolayer MoS_2*, J. Phys. Chem. C **119**, 4294–4301 (2015).

16 A. Tuxen, J. Kibsgaard, H. Gøbel, E. Lægsgaard, H. Topsøe, J. V. Lauritsen, and F. Besenbacher, *Size Threshold in the Dibenzothiophene Adsorption on MoS_2 Nanoclusters*, ACS Nano **4**, 4677–4682 (2010).

17 A. Bruix, H. G. Füchtbauer, A. K. Tuxen, A. S. Walton, M. Andersen, S. Porsgaard, F. Besenbacher, B. Hammer,

and J. V. Lauritsen, *In Situ Detection of Active Edge Sites in Single-Layer MoS_2 Catalysts*, ACS Nano **9**, 9322–9330 (2015).

18 S. Ding, S. Jiang, Y. Zhou, Q. Wei, and W. Zhou, *Catalytic Characteristics of Active Corner Sites in Co-Mo-S Nanostructure Hydrodesulfurization – A Mechanism Study Based on DFT Calculations*, J. Catal. **345**, 24–38 (2017).

19 S. Wang, Y. Rong, Y. Fan, M. Pacios, H. Bhaskaran, K. He, and J. H. Warner, *Shape Evolution of Monolayer MoS_2 Crystals Grown by Chemical Vapor Deposition*, Chem. Mater. **26**, 6371–6379 (2014).

20 J. V. Lauritsen, J. Kibsgaard, S. Helveg, H. Topsøe, B. S. Clausen, E. Lægsgaard, and F. Besenbacher, *Size-Dependent Structure of MoS_2 Nanocrystals*, Nat. Nanotechnol. **2**, 53–58 (2007).

21 Y. Shi, J.-K. Huang, L. Jin, Y.-T. Hsu, S. F. Yu, L.-J. Li, and H. Y. Yang, *Selective Decoration of Au Nanoparticles on Monolayer MoS_2 Single Crystals*, Sci. Rep. **3**, 1839 (2013).

22 P. H. Joo, J. Cheng, and K. Yang, *Size Effects and Odd-Even Effects in MoS_2 Nanosheets: First-Principles Studies*, Phys. Chem. Chem. Phys. **19**, 29927–29933 (2017).

23 A. K. Tuxen, H. G. Füchtbauer, B. Temel, B. Hinnemann, H. Topsøe, K. G. Knudsen, F. Besenbacher, and J. V. Lauritsen, *Atomic-Scale Insight into Adsorption of Sterically Hindered Dibenzothiophenes on MoS_2 and Co-Mo-S Hydrotreating Catalysts*, J. Catal. **295**, 146–154 (2012).

24 F. L. Deepak, A. Mayoral, and M. J. Yacaman, *Faceted MoS_2 Nanotubes and Nanoflowers*, Mater. Chem. Phys. **118**, 392–397 (2009).

25 B. G. Rao, H. S. S. R. Matte, P. Chaturbedy, and C. N. R. Rao, *Hydrodesulfurization of Thiophene Over Few-Layer MoS_2 Covered with Cobalt and Nickel Nanoparticles*, ChemPlusChem **78**, 419–422 (2013).

26 X. Dai, K. Du, Z. Li, M. Liu, Y. Ma, H. Sun, X. Zhang, and Y. Yang, *Co-Doped MoS_2 Nanosheets with the Dominant CoMoS Phase Coated on Carbon as an Excellent Electrocatalyst for Hydrogen Evolution*, ACS Appl. Mater. Interfaces **7**, 27242–27253 (2015).

27 Y. Guo, J. Tang, H. Qian, Z. Wang, and Y. Yamauchi, *One-Pot Synthesis of Zeolitic Imidazolate Framework 67-Derived Hollow Co_3S_4@MoS_2 Heterostructures as Efficient Bifunctional Catalysts*, Chem. Mater. **29**, 5566–5573 (2017).

28 F. Niefind, W. Bensch, M. Deng, L. Kienle, J. Cruz-Reyes, and J. M. D. V. Granados, *Co-Promoted MoS_2 for Hydrodesulfurization: New Preparation Method of MoS_2 at Room Temperature and Observation of Massive Differences of the Selectivity Depending on the Activation Atmosphere*, Appl. Catal. A: Gen. **497**, 72–84 (2015).

29 L. S. Byskov, J. K. Nørskov, B. S. Clausen, and H. Topsøe, *DFT Calculations of Unpromoted and Promoted MoS_2-Based Hydrodesulfurization Catalysts*, J. Catal. **187**, 109–122 (1999).

30 J. V. Lauritsen, J. Kibsgaard, G. H. Olesen, P. G. Moses, B. Hinnemann, S. Helveg, J. K. Nørskov, B. S. Clausen, H. Topsøe, E. Lægsgaard, and F. Besenbacher, *Location and Coordination of Promoter Atoms in Co- and Ni-Promoted MoS_2-Based Hydrotreating Catalysts*, J. Catal. **249**, 220–233 (2007).

31 S. Rangarajan and M. Mavrikakis, *On the Preferred Active Sites of Promoted MoS_2 for Hydrodesulfurization with Minimal Organonitrogen Inhibition*, ACS Catal. **7**, 501–509 (2017).

32 H. Wang, C. Tsai, D. Kong, K. Chan, F. Abild-Pedersen, J. K. Nørskov, and Y. Cui, *Transition-Metal Doped Edge Sites in Vertically Aligned MoS_2 Catalysts for Enhanced Hydrogen Evolution*, Nano Research **8**, 566–575 (2015).

33 M. Šarić, J. Rossmeisl, and P. G. Moses, *Modeling the Active Sites of Co-Promoted MoS_2 Particles by DFT*, Phys. Chem. Chem. Phys. **19**, 2017–2024 (2017).

34 G. Kresse and D. Joubert, *From Ultrasoft Pseudopotentials to the Projector Augmented-Wave Method*, Phys. Rev. B **59**, 1758–1775 (1999).

35 G. Kresse and J. Furthmüller, *Efficiency of Ab-Initio Total Energy Calculations for Metals and Semiconductors Using a Plane-Wave Basis Set*, Comput. Mater. Sci. **6**, 15–50 (1996).

36 P. E. Blöchl, *Projector Augmented-Wave Method*, Phys. Rev. B **50**, 17953–17979 (1994).

37 J. P. Perdew, K. Burke, and M. Ernzerhof, *Generalized Gradient Approximation Made Simple*, Phys. Rev. Lett. **77**, 3865–3868 (1996).

38 S. Grimme, J. Antony, S. Ehrlich, and H. Krieg, *A Consistent and Accurate Ab initio Parametrization of Density Functional Dispersion Correction (DFT-D) for the 94 Elements H-Pu*, J. Chem. Phys. **132**, 154104 (2010).

39 W. H. Miller, W. L. Hase, and C. L. Darling, *A simple model for correcting the zero point energy problem in classical trajectory simulations of polyatomic molecules*, J. Chem. Phys. **91**, 2863–2868 (1989).

40 A. P. Scott and L. Radom, *Harmonic Vibrational Frequencies: An Evaluation of Hartree-Fock, Møller-Plesset, Quadratic Configuration Interaction, Density Functional Theory, and Semiempirical Scale Factors*, J. Phys. Chem. **100**, 16502–16513 (1996).

41 A. S. Walton, J. V. Lauritsen, H. Topsøe, and F. Besenbacher, *MoS_2 Nanoparticle Morphologies in Hydrodesulfurization Catalysis Studied by Scanning Tunneling Microscopy*, J. Catal. **308**, 306–318 (2013).

42 Y. Zhu, Q. M. Ramasse, M. Brorson, P. G. Moses, L. P. Hansen, C. F. Kisielowski, and S. Helveg, *Visualizing*

the Stoichiometry of Industrial-Style Co-Mo-S Catalysts with Single-Atom Sensitivity, Angew. Chem. Int. Ed. **53**, 10723–10727 (2014).

43 S. S. Grønborg, N. Salazar, A. Bruix, J. Rodríguez-Fernández, S. D. Thomsen, B. Hammer, and J. V. Lauritsen, *Visualizing Hydrogen-Induced Reshaping and Edge Activation in MoS_2 and Co-Promoted MoS_2 Catalyst Clusters*, Nat. Commun. **9**, 2211 (2018).

44 J. V. Lauritsen and F. Besenbacher, *Atom-Resolved Scanning Tunneling Microscopy Investigations of Molecular Adsorption on MoS_2 and CoMoS Hydrodesulfurization Catalysts*, J. Catal. **328**, 49–58 (2015).

45 S. Marzooghi, B. E. Finch, W. A. Stubblefield, and D. M. Di Toro, *Predicting Phototoxicity of Alkylated PAHs, Mixtures of PAHs, and Water Accommodated Fractions (WAF) of Neat and Weathered Petroleum with the Phototoxic Target Lipid Model*, Environ. Toxicol. Chem. **37**, 2165–2174 (2018).

46 D. D. Wagman, W. H. Evans, V. B. Parker, R. H. Schumm, I. Halow, S. M. Bailey, K. L. Churney, and R. L. Nuttall, *Erratum: The NBS tables of chemical thermodynamic properties. Selected values for inorganic and C_1 and C_2 organic substances in SI units [J. Phys. Chem. Ref. Data 11, Suppl. 2 (1982)]*, J. Phys. Chem. Ref. Data **18**, 1807 – 1812 (1989).

47 R. D. Chirico, S. E. Knipmeyer, A. Nguyen, and W. V. Steele, *The Thermodynamic Properties of Dibenzothiophene*, J. Chem. Thermodyn. **23**, 431–450 (1991).

48 R. D. Chirico, S. E. Knipmeyer, A. Nguyen, and W. V. Steele, *The Thermodynamic Properties of Biphenyl*, J. Chem. Thermodyn. **21**, 1307–1331 (1989).

49 J. K. Nørskov, T. Bligaard, A. Logadottir, J. R. Kitchin, J. G. Chen, S. Pandelov, and U. Stimming, *Trends in the Exchange Current for Hydrogen Evolution*, J. Electrochem. Soc. **152**, J23 – J26 (2005).

50 J. K. Nørskov, B. S. Clausen, and H. Topsøe, *Understanding the trends in the hydrodesulfurization activity of the transition metal sulfides*, Catal. Lett. **13**, 1 – 8 (1992).

51 P. Sabatier, *Catalysis in Organic Chemistry* (D. Van Nostrand Company, 1913).

52 A. J. Medford, A. Vojvodic, J. S. Hummelshøj, J. Voss, F. Abild-Pedersen, F. Studt, T. Bligaard, A. Nilsson, and J. K. Nørskov, *From the Sabatier Principle to a Predictive Theory of Transition-Metal Heterogeneous Catalysis*, J. Catal. **328**, 36–42 (2015).

53 H. Orita, K. Uchida, and N. Itoh, *A Volcano-Type Relationship Between the Adsorption Energy of Thiophene on Promoted MoS_2 Cluster-Model Catalysts and the Experimental HDS Activity: Ab Initio Density Functional Study*, Appl. Catal. A: Gen. **258**, 115–120 (2004).

54 C. Xu and Q. Shi, *Structure and Modeling of Complex Petroleum Mixtures*, Structure and Bonding (Springer International Publishing, 2015).

55 H. Qi, D. Li, C. Yang, Y. Ma, W. Li, Y. Sun, and B. Zhong, *Nickel and manganese co-modified K/MoS_2 catalyst: high performance for higher alcohols synthesis from CO hydrogenation*, Catal. Commun. **4**, 339–342 (2003).

56 J. Sollner, D. F. Gonzalez, J. H. Leal, T. M. Eubanks, and J. G. Parsons, *HDS of Dibenzothiophene with $CoMoS_2$ Synthesized Using Elemental Sulfur*, Inorganica Chim. Acta **466**, 212–218 (2017).

57 B. Yoosuk, J. H. Kim, C. Song, C. Ngamcharussrivichai, and P. Prasassarakich, *Highly Active MoS_2, $CoMoS_2$ and $NiMoS_2$ Unsupported Catalysts Prepared by Hydrothermal Synthesis for Hydrodesulfurization of 4,6-Dimethyldibenzothiophene*, Catal. Today **130**, 14–23 (2008).

58 C. Geantet, J. De Los Reyes, M. Cattenot, M. Vrinat, M. Breysse, and S. Gőbölös, *Ruthenium molybdenum sulphide catalysts: physicochemical characterization and catalytic properties in HDS, hydrogenation and HDN reactions*, Catal. Today **10**, 665–680 (1991).

59 T. He, L. Xu, Y. Zhang, H. Huang, and H. Jiao, *High-quality vanadium-doped MoS_2 ultrathin nanosheets as an efficient ORR catalyst*, New J. Chem. **43**, 1611–1616 (2019).

60 V. Shokhen and D. Zitoun, *Platinum-Group Metal Grown on Vertically Aligned MoS_2 as Electrocatalysts for Hydrogen Evolution Reaction*, Electrochim. Acta **257**, 49–55 (2017).

Graphic Abstract

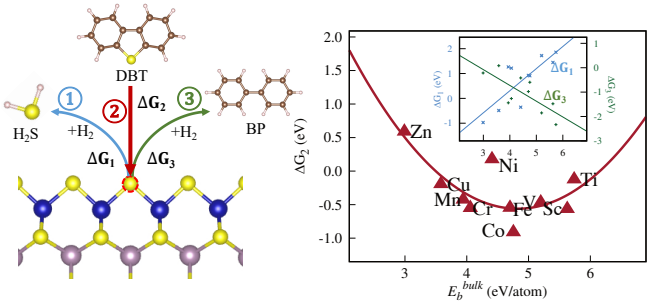

Table of Contents

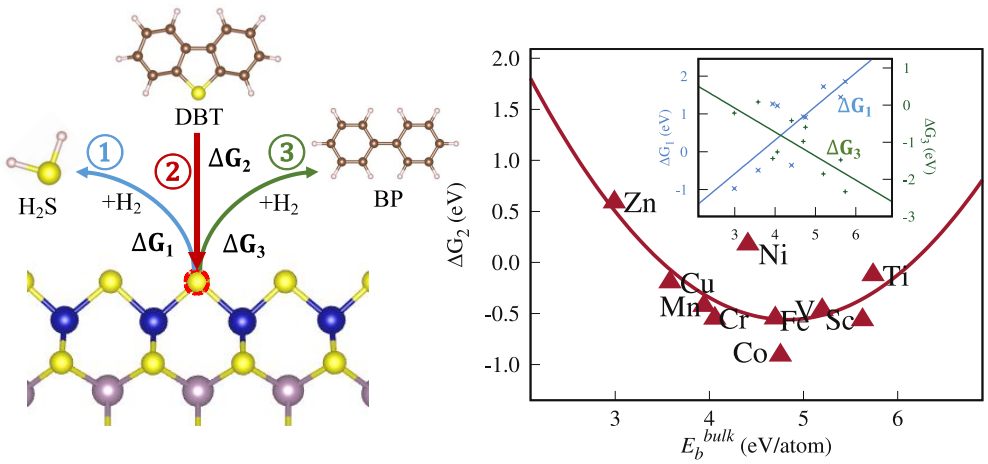

This work reports an effective descriptor for selecting appropriate transition-metal promoters for MoS_2-based nanocatalysts for hydrodesulfurization.